Inorg. Chem. **2006**, *45*, 2531–2542

Orbital Interactions in Fe(II)/Co(III) Heterobimetallocenes: Single versus Double Bridge

Ralf Warratz, Gerhard Peters, Felix Studt, René-Hermann Römer, and Felix Tuczek*

Institut für Anorganische Chemie, Christian Albrechts Universität Kiel, Otto Hahn Platz 6/7, D-24098 Kiel, Germany

Received October 19, 2005

Ferrocenyl cobaltocenium hexafluorophosphate (**1**) and ferrocenylene cobaltocenylenium hexafluorophosphate (**2**) are investigated by a range of spectroscopic methods. Both compounds are diamagnetic, in contrast to an earlier report indicating a temperature-dependent paramagnetism of **2**. Electronic absorption spectra of **1** and **2** are presented and fully assigned up to 50 000 cm^{-1} on the basis of electronic structure (DFT) calculations and spectral comparisons with ferrocene and cobaltocenium. The lowest-energy bands, I, of both **1** and **2** correspond to metal-to-metal CT (MMCT) transitions; further intermetallocene charge-transfer bands are identified at higher energy (bands III and V). On the basis of the spectroscopic properties, a trans geometry and a twisted structure are derived for **1** and **2**, respectively, in solution. Analysis of the I bands gives orbital mixing coefficients, α, electronic-coupling matrix elements, V_{AB}, and reorganization energies, λ. Importantly, α and V_{AB} are larger for **1** than for **2** (0.07 and 1200 cm^{-1} vs 0.04 and $\sim$600 cm^{-1}, respectively), apparently in contrast to the presence of one bridge in **1** and two bridges in **2**. This result is explained in terms of the respective electronic and geometric structures. Reorganization energies are determined to be 7600 cm^{-1} for **1** and 4600 cm^{-1} for **2**, in qualitative agreement with the analogous Fe(II)–Fe(III) compounds. The general implications of these findings with respect to the spectroscopic and electron-transfer properties of bimetallocenes are discussed.

I. Introduction

Mixed-valent (MV) bimetallocenes and heterobimetallocenes have been of continuing interest as model systems for the study of electron transfer.[1] One of the most fascinating phenomena associated with this class of compounds is the thermally driven charge localization−delocalization transition of ferrocene ferrocenium dimers which can be monitored by variable-temperature Mössbauer spectroscopy.[2] Diethylbiferrocenium triiodide, for example, is charge localized at low temperatures, exhibiting two discrete quadrupole doublets for Fe(II) and Fe(III). At a characteristic transition temperature, $T_c = 275$ K, it becomes charge delocalized, as evident from the appearance of a single quadrupole doublet.[3] No line broadening is observed in the intermediate temperature range which indicates that electronic relaxation is always fast on the Mössbauer time scale.[4] These phenomena have been interpreted on the basis of various theoretical approaches.[5,6,7] The most comprehensive physical description is provided by the vibronic model of Varret and co-workers which has been further elaborated by Klokishner et al.[8] This

* To whom correspondence should be addressed. E-mail: ftuczek@ac.uni-kiel.de.

(1) Barlow, S.; O'Hare, D. *Chem. Rev.* **1997**, *97*, 637. (b) Hendrickson, D. N. *NATO ASI Ser., Ser. C* **1991**, *343*, 67. (c) Sano, H. *Hyperfine Interact.* **1990**, *53*, 97. (d) Dong, T.-Y.; Chang, L.-S.; Lee, G.-H.; Peng, S.-M. *Organometallics*, **2002**, *21*, 4192. (e) Oda, T.; Nakashima, S.; Okuda, T. *Inorg. Chem.* **2003**, *42*, 5376. (f) Morrison, W. H., Jr.; Hendrickson, D. N. *Inorg. Chem.* **1975**, *14*, 2331. (g) Jones, S. C.; Barlow, S.; O'Hare, D. *Chem.—Eur. J.* **2005**, *11*, 4473. (h) Richardson, D. E.; Taube, H. *Coord. Chem. Rev.* **1984**, *60*, 107.

(2) Dong, T.-Y.; Hendrickson, D. N.; Iwai, K.; Cohn, M. J.; Geib, S. J.; Rheingold, A. L.; Sano, H.; Motoyama, I.; Nakashima, S. *J. Am. Chem. Soc.* **1985**, *107*, 7996. (b) Webb, R. J.; Dong, T. Y.; Pierpont, C. G.; Boone, S. R.; Chadha, R. K.; Hendrickson, D. N. *J. Am. Chem. Soc.* **1991**, *113*, 4806. (c) Dong, T. Y.; Huang, C.-H.; Chang, C.-K.; Wen, Y. S.; Lee, S.-L.; Chen, J.-A.; Yeh, W.-Y.; Yeh, A. *J. Am. Chem. Soc.* **1993**, *115*, 6357.

(3) Iijiama, S.; Saida, R.; Motoyama, I.; Sano, H. *Bull. Chem. Soc. Jpn.* **1981**, *54*, 1375. (b) Nakashima, S.; Nishimori, A.; Masuda, Y.; Sano, H.; Sorai, M. *J. Phys. Chem. Solids* **1991**, *52*, 1169.

(4) Boukheddaden, K.; Linares, J.; Varret, F. *Phys. Rev. B* **1993**, *47*, 14070.

(5) Dong, T.-Y.; Hendrickson, D. N.; Iwai, K.; Cohn, M. J.; Geib, S. J.; Rheingold, A. L.; Sano, H.; Motoyama, I.; Nakashima, S. *J. Am. Chem. Soc.* **1985**, *107*, 7996.

(6) Kambara, T.; Hendrickson, D. N.; Dong, T.-Y.; Cohn, M. J. *J. Chem. Phys.* **1987**, *86*, 2362.

(7) Boukheddaden, K.; Linares, J.; Varret, F. *Phys. Rev. B.* **1994**, *49*, 15659.

(8) Klokishner, S.; Linares, J.; Varret, F. *Chem. Phys.* **1998**, *226*, 171.

10.1021/ic051809l CCC: $33.50
Published on Web 02/25/2006

treatment attributes the charge localization−delocalization transitions to cooperative interactions between the bimetallocene molecules in the crystalline solid which modulate the energy difference, W_d, between the minima of the double-well potentials of the individual dimers. At low temperatures, these potentials are asymmetric, and W_d is large compared to kT, corresponding to a charge-ordered state. Upon an increase of the temperature, W_d decreases, eventually becoming zero at T_c. The situation at this temperature and above thus corresponds to a symmetrical class II mixed-valent dimer (according to the Robin and Day classification scheme),[9] leading to a charge-averaged state in the presence of fast relaxation.

The cooperative interactions determining T_c sensitively depend on the substituents[2] and the counterions[10] of the $FcFc^+$ dimers. To systematically modify these interactions and thus obtain further information on their physical nature, we are planning to dilute the ferrocene−ferrocenium ($FcFc^+$) dimers in a matrix of the analogous ferrocene−cobaltocenium ($FcCc^+$) compounds and investigate the charge localization−delocalization transitions of the resulting *mixed* systems. The present paper is a first step in this direction, dealing with the electronic structure of neat Fe(II)/Co(III) heterobimetallocenes. To this end, we investigate the two compounds ferrocenyl cobaltocenium hexafluorophosphate ($FcCcPF_6$, **1**) and ferrocenylene cobaltocenylenium hexafluorophosphate ($BFFeCoPF_6$, **2**),[11] containing singly (**1**) and doubly bridged (**2**) ferrocene/cobaltocenium units. These heterobimetallic MV molecules, composed of two closed-shell d^6-d^6 metal centers, should be inactive with respect to electron transfer (i.e., the Fe(II) → Co(III) metal-to-metal charge-transfer (MMCT) state should be thermally inaccessible with respect to the electronic ground state, at least below 300 K). In this respect it is noteworthy that compound **2** was reported to be paramagnetic.[12,13] Magnetic moments of $\mu_{eff} = 2.37$ and 1.03 μ_B at 295 and 77 K, respectively, were determined using a Gouy balance. This was interpreted in terms of a temperature-dependent Fe(II)−Co(III) ↔ Fe(III)−Co(II) charge averaging process.[12] The paramagnetism was also invoked to explain that a ^{1}H NMR spectrum of **2** could not be obtained. Further support for the assumption of a valence-averaged system was derived from the crystal structure of $BFFeCoPF_6$ which exhibits a remarkably similar lattice compared to that of the analogous, valence-delocalized Fe(II)−(III) compound[13] and from the fact that electronic-coupling phenomena have also been observed in other members of the bisfulvalene dimetal family.[14]

The singly bridged bimetallocene $FcCcPF_6$ (**1**) and the analogous dibridged complex, $BFFeCoPF_6$ (**2**), were synthesized according to published routes[12,15] and investigated with a range of spectroscopic methods. In terms of the Robin and Day classification scheme,[9] ferrocene−ferrocenium dimers are class II MV compounds which exhibit intense and broad intervalence charge-transfer (IVCT) transitions[16] in the VIS or NIR region of the absorption spectrum.[17] Similar low-energy metal → metal charge-transfer (MMCT) transitions should be observable for the Fe(II)/Co(III) heterodimetal compounds **1** and **2**. It is known that **1** is solvatochromic,[12] but (as for **2**) no visible spectra have been reported. A major goal of this study is therefore to present and interpret these spectra, with particular emphasis on the Fe(II) → Co(III) MMCT transitions. The corresponding band positions, intensities, and widths are analyzed on the basis of the Hush formulas,[18] and orbital mixing coefficients, α, electronic-coupling matrix elements, V_{AB}, and reorganization energies, λ, are determined for **1** and **2**. These spectroscopic results are correlated to the electronic structures of both compounds which are determined by DFT calculations, and the general implications with respect to electron-transfer phenomena in bimetallocenes are discussed.

II. Results and Analysis

NMR, Mössbauer, and Magnetic Characterization of 1 and 2. The ^{1}H NMR parameters of ferrocenyl cobaltocenium hexafluorophosphate ($FcCcPF_6$, **1**) have been reported before.[15] Well-resolved ^{1}H and ^{13}C NMR spectra[19] could also be obtained for ferrocenylene cobaltocenylenium hexafluorophosphate ($BFFeCoPF_6$, **2**), in contrast to an earlier report.[12] This suggests that **2** is diamagnetic, analogous to **1**. Mössbauer spectra of **1** and **2** were recorded at 300 K and low temperatures.[20] Quadrupole splittings of $\Delta E_Q = 2.20$ mm/s at 300 K and 2.27 mm/s at 10 K, as well as 2.47 mm/s at 300 and 80 K, have been found for **1** and **2**, respectively. Isomeric shifts and their temperature dependence are typical for this class of compounds.[21] The Mössbauer data thus indicate the presence of an Fe(II) low-spin state, as for other ferrocene derivatives.[22,23] Magnetic measurements on purified samples of **2** on a Faraday balance showed no detectable temperature-dependent magnetic moment within the temperature range of 300−100 K.

The combined NMR, Mössbauer, and magnetic susceptibility data thus confirm an Fe(II)−Co(III) d^6-d^6 closed-shell electronic ground state of **2**, well isolated from the Fe(II) high-spin or Fe(III)−Co(II) MMCT excited states; the same applies to **1**. Further details are given in the Supporting Information.[19,20]

(9) Robin, M. B.; Day, P. *Adv. Inorg. Chem. Radiochem.* **1967**, *10*, 247.
(10) Dong, T.-Y.; Kambara, T.; Hendrickson, D. N. *J. Am. Chem. Soc.* **1986**, *108*, 5857. (b) Dong, T.-Y.; Kambara, T.; Hendrickson, D. N. *J. Am. Chem. Soc.* **1986**, *108*, 4423.
(11) This acronym is based on the bisfulvalene nomenclature.
(12) Schwarzhans, K. E.; Schottenberger, H. *Z. Naturforsch.* **1983**, *38b*, 1493.
(13) Brüggeler, P.; Jaitner, P.; Schottenberger, H.; Schwarzhans, K. E. *J. Organomet. Chem.* **1991**, *417*, C53.
(14) The neutral divanadium bisfulvalene complex, for example, is diamagnetic, whereas the parent vanadocene has three unpaired electrons: Smart, J. C.; Pinsky, B. L. *J. Am. Chem. Soc.* **1980**, *102*, 1009. The same holds for the diamagnetic bisfulvalene diiron dication formally containing two d^5 iron centers: ref 22.
(15) Schwarzhans, K. E.; Stolz, W. *Monatsh. Chem.* **1978**, *118*, 875.
(16) Allen, G. C.; Hush, N. S. *Prog. Inorg. Chem.* **1967**, *8*, 391.
(17) Cowan, D. O.; LeVanda, C. *J. Am. Chem. Soc.* **1972**, *94*, 9271.
(18) Hush, N. S. *Prog. Inorg. Chem.* **1967**, *8*, 391.
(19) See Figures S1−S3 in the Supporting Information for these spectra and a more detailed discussion of the NMR data.
(20) See Figure S4, as well as Table S1, in the Supporting Information.
(21) Fluck, E.; Hausser, F. *Z. Anorg. Allg. Chem.* **1973**, *396*, 257.
(22) Le Vanda, C.; Bechgaard, K.; Cowan, D. O.; Müller-Westhoff, U. T.; Eilbracht, P.; Candela, G. A.; Collins, R. L. *J. Am. Chem. Soc.* **1976**, *98*, 3181.
(23) Wertheim, G. K.; Herber, R. H. *J. Chem. Phys.* **1963**, *38*, 2106.

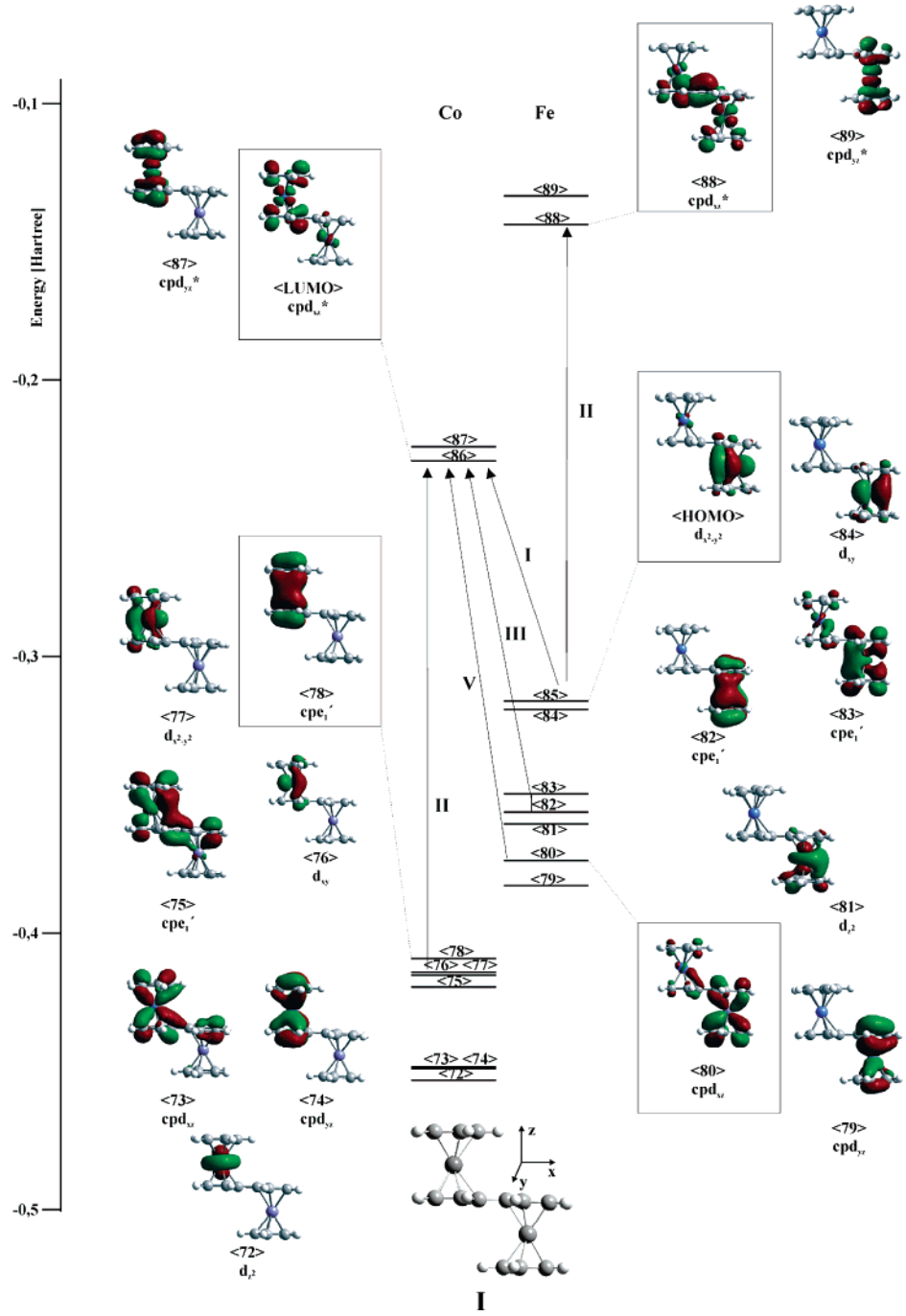

Figure 1. Molecular orbital scheme of FcCcPF6 (**1**) based on the optimized structure FcCc+ (**I**) along with internal coordinates. Arrows show the possible transitions within the dimer from bands I−III and V (bands IV and VI are omitted for clarity).

Electronic Structures. More information on the electronic structures of **1** and **2** is obtained through a combination of optical absorption spectroscopy and DFT calculations performed on models **I** and **II**, respectively. A section of the MO scheme of optimized structure **I** containing all orbitals with significant metal d contribution is given in Figure 1. The coordinate system is oriented such that the *x* axis is along the central C−C bond of the fulvalenide ligand and the *z* axis is perpendicular to the ligand plane. The HOMO and HOMO−1 of **I** are the nearly degenerate, predominantly iron-centered orbitals $d_{x^2-y^2}$ and d_{xy} (⟨84⟩ and ⟨85⟩), followed at lower energy by a set of ligand functions (cpe$_1$′),[24] the Fe d_{z^2} orbital, and the metal−ligand bonding combinations of Fe d_{xz} and d_{yz}, cpd_{xz} and cpd_{yz}. Below these orbitals (all of which are centered at the ferrocene subunit), the highest-occupied orbital of the cobaltocenium moiety, one member of the cpe$_1$′ set of ligand-type orbitals, is found. At even lower energy, the almost degenerate Co $d_{x^2-y^2}$ and d_{xy} functions are located. These four orbitals, completed by the second cpe$_1$′ ligand-type function, are closely spaced in energy. The lowest MOs of the cobaltocenium moiety

(24) The orbital designations are derived from those of the isolated subunits ferrocene and cobaltocenium, respectively, having D_{5h} symmetry (cf. Supporting Information Figures S7 and S8).

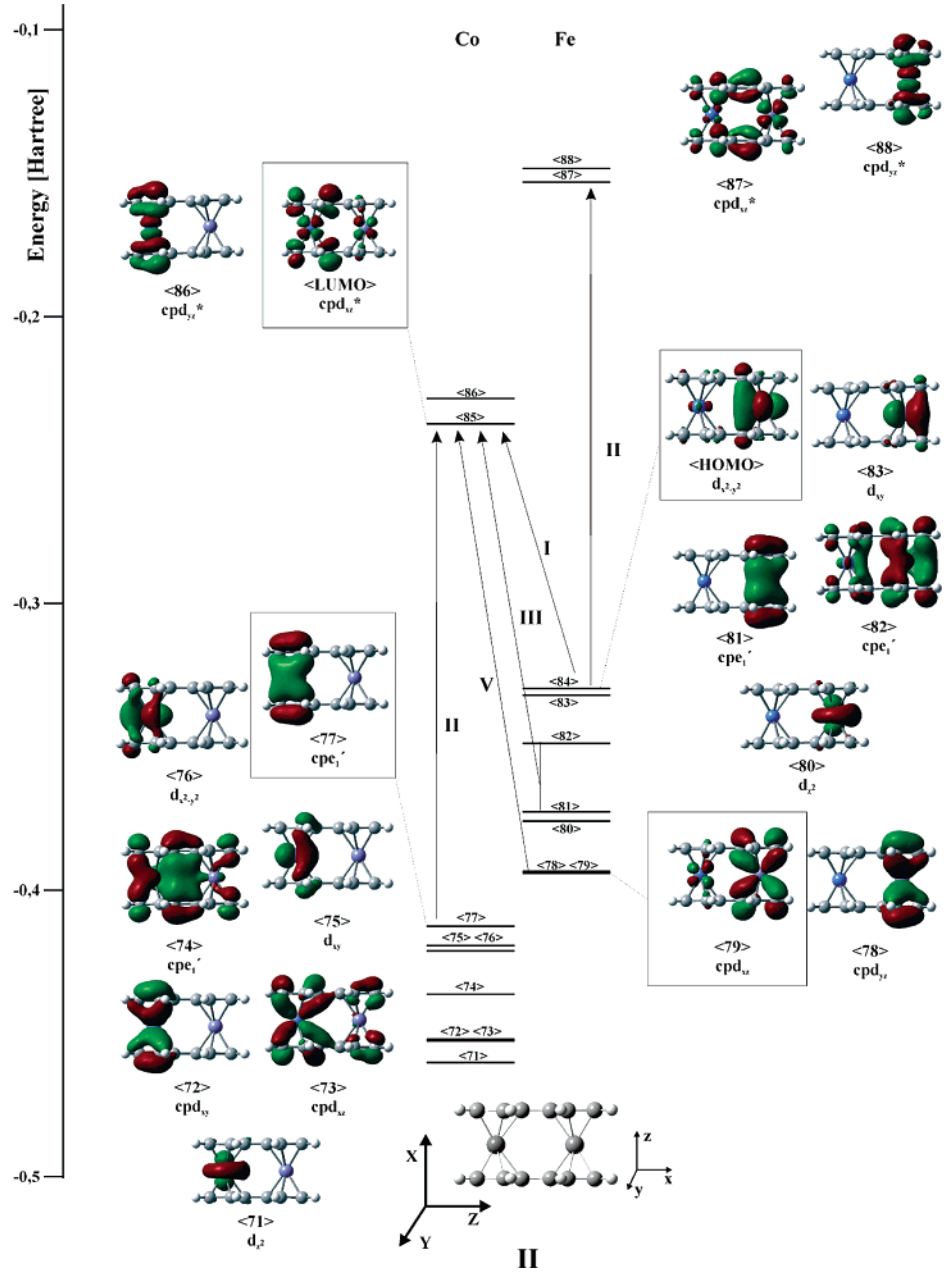

Figure 2. Molecular orbital scheme of BFFeCoPF6 (**2**) based on the optimized structure BFFeCo+ (**II**) along with internal and molecular coordinates. Arrows show the possible transitions within the dimer arising from bands I−III and V (bands IV and VI are omitted for clarity).

considered here are the quasidegenerate set of cpd$_{xz}$ and cpd$_{yz}$ metal−ligand bonding orbitals and the Co d$_{z^2}$ orbital.

The LUMO and LUMO+1 of **1** are formed by the metal−ligand antibonding combinations cpd$_{xz}$* and cpd$_{yz}$* of the cobaltocenium subunit, ⟨86⟩ and ⟨87⟩, respectively. On the ferrocene side, the analogous combinations correspond to LUMO+2 and LUMO+3 (⟨88⟩ and ⟨89⟩, respectively). Therefore, the MO scheme of the ferrocenyl cobaltocenium dimer **I** can be considered to be a superposition of the MO schemes of ferrocene and cobaltocenium (which are very similar to each other; cf., Supporting Information for the molecular orbital schemes), with all cobaltocenium functions (occupied and unoccupied) shifted to lower energy because of the higher effective nuclear charge of the central atom.[25] As on both subunits, three metal-type orbitals (i.e., d$_{z^2}$, d$_{xy}$, and d$_{x^2-y^2}$) are occupied and two metal-type orbitals (i.e., d$_{xz}$ and d$_{yz}$) are unoccupied, a d^6−d^6 low-spin Fe(II)−Co(III) configuration results, in full agreement with the experimental results.

The MO scheme of **2**, based on the optimized structure (**II**) of its cation, shows that the addition of the second bridge leaves this overall picture more or less unaffected (Figure 2). The orientation of *x*, *y*, and *z* in **II** is analogous to that in **I**; for further reference, we also define a molecular coordinate system with X in the fulvalenide−fulvalenide and Z in the metal−metal direction. The HOMO and HOMO−1 of **II** are again the iron-centered orbitals d$_{x^2-y^2}$ ⟨83⟩ and d$_{xy}$ ⟨84⟩, which

(25) The low-energy shift of the Co orbitals is more pronounced, the higher the metal character is. The HOMO of the cobaltocenium unit is therefore calculated to be of ligand type.

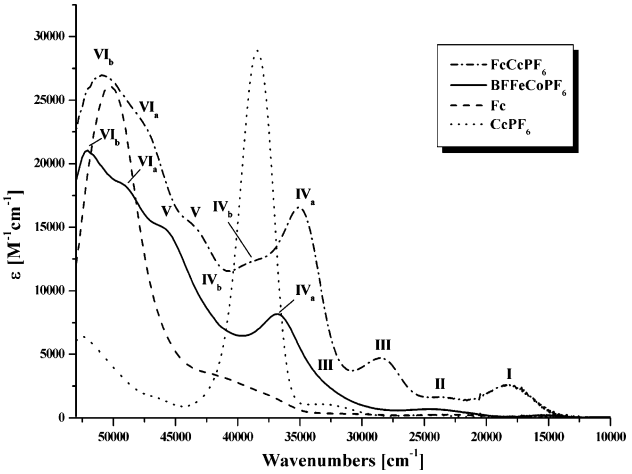

Figure 3. UV-vis spectra of FcCcPF6 (**1**) and BFFeCoPF6 (**2**), along with those of the parent compounds, ferrocene (Fc) and cobaltocenium hexafluorophosphate (CcPF6). See text for band assignments.

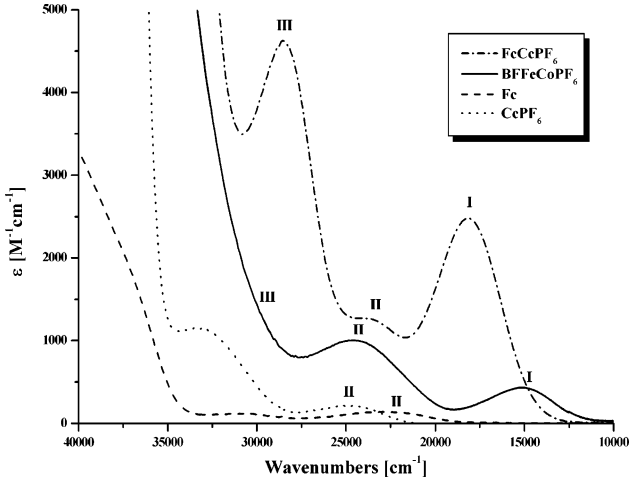

Figure 4. Detailed plot of the UV−vis low-energy region of FcCcPF6 (**1**) and BFFeCoPF6 (**2**), along with those of the parent compounds, ferrocene (Fc) and cobaltocenium hexafluorophosphate (CcPF6). See text for band assignments.

are close to degenerate. At lower energy, ligand-type MOs corresponding to the ferrocene cpe_1' orbitals are located (HOMO−2, HOMO−3). HOMO−4 represents the iron-centered d_{z^2} orbital, whereas the bonding combinations of the bisfulvalenide orbitals with the iron d_{xz} and d_{yz} orbitals are almost degenerate, forming HOMO−5 and HOMO−6. Below these mainly ferrocene-type orbitals, the cobalt-centered functions are located, the energetic sequence of which is slightly different. In particular, the Co(III) d orbitals are shifted to lower energy than the cpe_1' ligand orbitals, such that one of the latter orbitals is at highest energy (vide supra). Moreover, the d_{z^2} orbital is at lower energy than the cpd_{xz} and cpd_{yz} metal−ligand bonding combinations.

The LUMO and LUMO+1 of **II** are the metal−ligand antibonding combinations of the Co d_{xz} and d_{yz} orbitals (⟨85⟩ and ⟨86⟩, respectively). Like their metal−ligand bonding counterparts, these orbitals are nearly degenerate; this also applies to the metal−ligand antibonding d_{xz} and d_{yz} orbitals of the iron subunit (LUMO+3 and LUMO+4). In summary, three metal-type orbitals (d_{z^2}, d_{xy}, and $d_{x^2-y^2}$) are occupied both in the iron and the cobalt subunit. The d_{xz} and d_{yz} orbitals of the metals interact with the bisfulvalenide ligands to form two (predominantly ligand-type) bonding combinations which are occupied and two (metal-type) antibonding combinations which are empty. Complex **2** therefore can be described by an Fe(II) d^6 Co(III) d^6 low-spin configuration, analogous to **1** and again in agreement with the experimental results.

Electronic Transitions. The MO schemes of **I** and **II** and the optical absorption spectra of ferrocene and cobaltocenium form the basis for a detailed analysis of the electronic transitions of **1** and **2**. Figure 3 gives the absorption spectra of $FcCcPF_6$ (**1**) and $BFFeCoPF_6$ (**2**) along with those of the constituent monomeric metallocenes, ferrocene and cobaltocenium hexafluorophosphate; a blow-up of the lower-energy region is shown in Figure 4. It should be mentioned that there are no further transitions at lower energy in the NIR region. Band positions and intensities are collected in Table 1. Table 2 contains results of time-dependent DFT (TDDFT) calculations together with assignments of the individual transitions. Although the absolute values of the theoretically determined transition energies differ appreciably from the experimental data, they provide information regarding the energetic sequence of the electronic transitions. Gaussian fit analysis of the spectra of **1** and **2** are presented in the Supporting Information.

Table 1. UV−Vis Data for $FcCcPF_6$ (**1**) and $BFFeCoPF_6$ (**2**), as well as for the Parent Compounds, Ferrocene (Fc) and Cobaltocenium hexafluorophosphate ($CcPF_6$)

	λ_{max}[nm] (ϵ_{max} [$M^{-1}cm^{-1}$])	
compound	acetonitrile	dichloromethane
$FcCcPF_6$	192 (33 000), 210 (25 000), 230 (15 500), 255 (1300), 284 (15 600), 347 (4650), 424 (1270), 552 (2480)	354 (4570), 425 (1200), 580 (2440)
$BFFeCoPF_6$	192 (21 000), 206 (18 000), 220 (14 500), 272 (8200), 412 (1000), 659 (420)	274 (8700), 405 (780), 691 (320)
Fc	199 (26 000), 237 (3550), 326 (70), 442 (90)	327(68), 442 (88)
$CcPF_6$	192 (6550), 217 (1674), 263 (30 000), 301 (1000), 404 (210)	302 (910), 405 (200)

The singly bridged compound, **1**, exhibits characteristic, intense colors in various solvents. The solvatochromism of this compound is already evident from the fact that the compound gives a blue solution in dichloromethane which turns purple when a more polar solvent is added. With respect to the constituent complexes, compound **1** most conspicuously exhibits two new absorption features at 18 115 cm^{-1} (552 nm, band I) and 28 782 cm^{-1} (347 nm, band III, acetonitrile solution), both of which exhibit solvatochromic behavior (cf. Figure 5). In contrast, there are other bands in the spectrum of **1** (i.e., band II) which are not solvatochromic and most likely correspond to transitions of the individual constituent metallocenes, ferrocene and cobaltocenium. At higher energy, ferrocene and cobaltocenium salts have intense absorption bands at 50 000 cm^{-1} (exhibiting two shoulders at 37 700 and 41 700 cm^{-1}) and 38 000 cm^{-1}, respectively, which have been assigned to transitions from the (metal−ligand nonbonding, ligand-type) cpe_1' orbitals to the (metal−

Table 2. Band Assignments and TDDFT Predictions for the Optimized Structures $FcCc^+$ (**I**) and $BFFeCo^+$ (**II**)

	$FcCC^+$ (**I**)			$BFFeCo^+$ (**II**)		
band	exptl energy (cm^{-1})	assignment	TDDFT energy (cm^{-1}) (oscillator strength)	exptl energy (cm^{-1})	assignment	TDDFT energy (cm^{-1}) (oscillator strength)
I	18 115	MMCT HOMO−LUMO	12 674 (0.0015)	15 174	MMCT HOMO−LUMO	∼10 000 (0)
II	23 181	intraMc−LF transitions	∼16 500 (0.0010) Fc ∼17 400−20 900 (0.0002−0.0034) Cc^+	24 813	intraMc−LF transitions	∼16 100 (0.0001) Fc ∼18 000−22 000 (0.0004) Cc^+
III	28 782	interMc−LMCT $cpe_1'^{Fe} \rightarrow$ LUMO	23 000 (0.0114)	34 055	interMc−LMCT $cpe_1'^{Fe} \rightarrow$ LUMO	18 900 (0.0003)
VI_a VI_b	34738 38 912	intraMc−LMCT $cpe_1'^{Co} \rightarrow$ LUMO	∼18 000 (0)	36 692 41 678	intraMc−LMCT $cpe_1'^{Co} \rightarrow$ LUMO	∼21 000 (0)
V	43 145	MMCT $cpd_{xz}^{Fe} \rightarrow$ LUMO	26 000 (0.0030)	45 734	MMCT $cpd_{xz}^{Fe} \rightarrow$ LUMO	28 900 (0.0078)
VI_a VI_b	46 895 51 572	intrMc−LMCT $cpe_1'^{Fe} \rightarrow$ LUMO+2	not calcd	49 641 52 675	intrMc−LMCT $cpe_1'^{Fe} \rightarrow$ LUMO+2	not calcd

ligand antibonding, metal-type) d_{xz} and d_{yz} orbitals (i.e., LMCT transitions).[26,27] These transitions appear at comparable energies in the spectrum of **1**, in agreement with the molecular orbital scheme shown in Figure 1 which indicates an energy difference of about 40 000 cm^{-1} between these orbitals (somewhat less for the Co unit, somewhat more for the Fe unit). However, both the ferrocene and cobaltocenium LMCT bands are split in the spectra of **1** and **2** because of the symmetry lowering in the dimer (cf. Figure 3). We assume that band IV_a located at about 34 740 cm^{-1} in **1** represents the lowest-energy component of this set of transitions. This feature and its counterpart IV_b located at somewhat higher energy (38 910 cm^{-1}) are assigned to the split LMCT transitions within the cobaltocenium subunit. Correspondingly, bands VI_a and VI_b located at 46 900 and 51572 cm^{-1}, respectively, are assigned to the ligand-to-metal transitions of the ferrocene subunit. Between bands IV and VI, at 42 130 cm^{-1}, is an additional feature (band V) which is attributed to a new transition within the dimer. On the basis of the molecular orbital scheme and TDDFT calculations (cf. Table 2), this band is assigned to an intermetallocene (interMc) transition from the occupied cpd_{xz}^{Fe} orbital into the empty $cpd_{xz}{}^{*Co}$ orbital, the LUMO of **1** (cf. Figure 1). Another interMc transition is associated with band III (vide supra), which on the basis of the MO scheme of **I** is assigned to the transition from the ferrocene ligand orbitals $cpe_1'^{Fe}$ to the cobaltocenium LUMO. The ferrocene-to-cobaltocenium charge-transfer character of this band is also evident from its solvatochromism (Figure 5). Solvatochromic behavior is also observed for the lowest-energy transitions of **1** (band I) which is assigned to transitions from the ferrocene-centered HOMO to the cobaltocenium-centered LUMO. This low-energy MMCT transition corresponds to the IVCT bands of homometallic MV dimers. The remaining band II can be attributed to ligand-field (LF) transitions within the ferrocene and the cobaltocenium subunits which obviously are little affected by the coupling of the two subunits (vide infra).

The absorption spectrum of the doubly bridged compound **2** is analyzed in a similar fashion. A new feature appears at 15 174 cm^{-1} (659 nm, acetonitrile solution) which is likely of the same origin as band I of **1** and is therefore denoted similarly. The presence of this absorption band is already evident from the fact that the color of $BFFeCoPF_6$ is deep green, whereas cobaltocenium hexafluorophosphate is yellow and ferrocene is yellow to orange. Further investigation of the absorption spectrum of **2** in different solvents reveals a slight solvatochromism of this band. A red-shift of about 700 cm^{-1} is observed, for example, upon changing the solvent from acetonitrile to dichloromethane. The higher-energy band II is in principle consistent with transitions of the individual parent metallocenes, slightly shifted in energy in the coupled system. Gaussian fit analysis (see Supporting Information) reveals the presence of an additional band at about 34 050 cm^{-1} which probably corresponds to band III in the spectrum of **1** and is assigned to the respective interMc transition from the iron to the cobalt moiety. Further transitions at 36 700 and 41 680 cm^{-1} are assigned to the split intrametallocene (cobaltocenium) LMCT transition bands, IV_a and IV_b. The same applies to bands VI_a and VI_b which are assigned to the corresponding ferrocene transitions. Band V at 45 740 cm^{-1}, finally, corresponds to a new

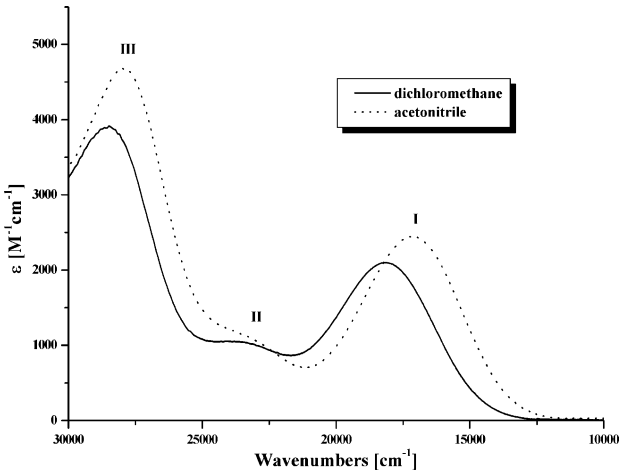

Figure 5. Solvatochromism of the low-energy bands I and III of FcCcPF6 (**1**) upon going from acetonitrile to dichloromethane.

(26) Sohn, Y. S.; Hendrickson, D. N.; Gray, H. B. *J. Am Chem. Soc.* **1971**, *93*, 3603.

(27) Like the ferrocene CT transition, this band has an additional shoulder (at ∼32 500 cm^{-1}).

transition within the dimer and is assigned to the $cpd_{xz}^{Fe} \rightarrow cpd_{xz}{}^{*Co}$ interMc transition, in analogy to **1**.

To conclude, the spectra of **1** and **2** can be fully assigned, based on the spectra of the constituent metallocenes and the MO schemes of **I** and **II**, respectively. Apart from the intrametallocene (intraMc) ligand-field transition II and the split intraMc LMCT transitions IV and VI, new intermetallocene (interMc) bands I, III, and V are identified for both **1** and **2** which in turn can be of MMCT (bands I and V) or of LMCT type (band III). Each of these interMc bands can be used to evaluate specific orbital interactions between the two metallocene subunits of **1** and **2**, as shown in the next section.

Evaluation of the Electronic Interaction (V_{ab}) and Orbital Mixing Coefficient (α) for 1. As an example, we analyze band I of compound **1** which is associated with the HOMO−LUMO transition. In the C_s symmetry of the optimized structure **I** (Figure 1), the $d_{x^2-y^2}$ and d_{xz} orbitals mix so that the Fe $d_{x^2-y^2}$-type HOMO has a contribution from the Co d_{xz}-type LUMO and vice versa[28,29]

$$\mathrm{HOMO} = \sqrt{1-\alpha^2}\,d_{x^2-y^2}{}^{Fe} - \alpha d_{xz}{}^{Co} \quad (1)$$

$$\mathrm{LUMO} = \sqrt{1-\alpha^2}\,d_{xz}{}^{Co} + \alpha d_{x^2-y^2}{}^{Fe} \quad (2)$$

The transition dipole matrix element between these two orbitals is approximately given by

$$\langle \mathrm{HOMO}|\mu|\mathrm{LUMO}\rangle = \sqrt{1-\alpha^2}\alpha(\langle d_{x^2-y^2}{}^{Fe}|\mu|d_{x^2-y^2}{}^{Fe}\rangle - \langle d_{xz}{}^{Co}|\mu|d_{xz}{}^{Co}\rangle) \approx \alpha r \quad (3)$$

with the metal−metal distance being denoted by r. The same holds for the HOMO−1 ⟨84⟩ and the LUMO+1 ⟨87⟩ (Fe d_{xy} and Co d_{yz}, respectively) both of which have A″ symmetry. In this case, however, ⟨84⟩ is totally localized on the Fe and ⟨87⟩ totally on the Co subunit (→α = 0) such that the transition dipole matrix element vanishes. Now, the electronic ground state is given by

$$\Psi^{GS} = |\,\overset{+}{\mathrm{HOMO}}\,\overset{-}{\mathrm{HOMO}}|\quad (4)$$

and the singlet HOMO−LUMO excited state by

$$\Psi^{ES} = \frac{1}{\sqrt{2}}\{|\overset{+}{\mathrm{HOMO}}\,\overset{-}{\mathrm{LUMO}}| - |\overset{-}{\mathrm{HOMO}}\,\overset{+}{\mathrm{LUMO}}|\} \quad (5)$$

such that

$$\langle Y^{GS}|\mu|\Psi^{ES}\rangle = \sqrt{2}\langle \mathrm{HOMO}|\mu|\mathrm{LUMO}\rangle = \sqrt{2}\alpha r \quad (6)$$

On the other hand, the intensity of band I is given by (Gaussian band shape)

$$I^{BandI} = \int_{BandI}\epsilon(\tilde{\nu})d\tilde{\nu} = 1.067\epsilon_{max}\Delta_{1/2} = |\langle\Psi^{GS}|\mu|\Psi^{ES}\rangle|^2 2.511\times10^3\tilde{\nu}_{max} = 2|\langle \mathrm{HOMO}|\mu|\mathrm{LUMO}\rangle|^2 2.511\times10^3\tilde{\nu}_{max} = 2\alpha^2 r^2 2.511\times10^3\tilde{\nu}_{max} \quad (7)$$

Scheme 1. Schematic Representation of the MO Schemes of a Closed- and Open-Shell M(II)−M(III) Mixed-Valent Dimer

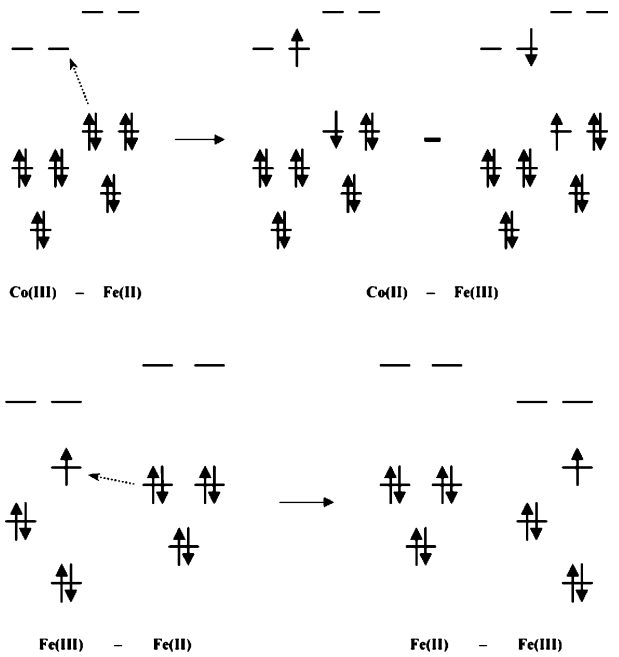

with the full width at half-maximum (fwhm), frequency (in wavenumbers), and maximum intensity (in units of M^{-1} cm^{-1}) of band I denoted by $\Delta_{1/2}$, $\tilde{\nu}_{max}$, and ϵ_{max}, respectively. Combining eqs 6 and 7 and solving for α yields

$$\sqrt{2}\alpha = 2.05\times10^{-2}\sqrt{\frac{\epsilon_{max}\Delta_{1/2}}{r^2\tilde{\nu}_{max}}} \quad (8)$$

or, with the electronic coupling matrix element, V_{AB}, between $d_{x^2-y^2}{}^{Fe}$ and $d_{xz}{}^{Co}$ being related to the orbital mixing coefficient, α, by

$$\alpha = \frac{|V_{AB}|}{\tilde{\nu}_{max}} = \frac{|H_{AB}|}{hc\tilde{\nu}_{max}} = \frac{|\langle d_{x^2-y^2}{}^{Fe}|H|d_{xz}{}^{Co}\rangle|}{hc\tilde{\nu}_{max}} \quad (9)$$

$$\sqrt{2}V_{AB} = 2.05\times10^{-2}\frac{\sqrt{\epsilon_{max}\Delta_{1/2}\tilde{\nu}_{max}}}{r} \quad (10)$$

These expressions differ from those given by Hush[18] by the factor $\sqrt{2}$ which derives from the fact that the excited state corresponds to a linear combination of two Slater determinants (eq 5, cf. Scheme 1). This is in contrast to an open-shell mixed-valent dimer where both involved states are single determinants and, upon the IVCT transition, the location of the SOMO shifts from one metal to the other. Similar to the IVCT state of a homometallic MV dimer, however, the HOMO−LUMO excited state of compound **1** has the same symmetry as the ground state and thus mixes with this state. In a valence-bond configuration interaction

(28) The orbital mixing coefficient, α, is defined as being positive; the particular phases in **1** and **2** derive from the fact that the two metallocene units are connected via the cp rings and not via a direct metal−metal interaction.

(29) It is assumed that the d^{Fe} and d^{Co} orbitals are admixed with ligand (cp) orbitals as in ferrocene and cobaltocenium, respectively (i.e., we are effectively considering subunit MOs).

(VBCI) type formalism,[30,31] the (unperturbed) Fe(III)−Co(II) singlet excited state is admixed with the coefficient $\sqrt{2}\alpha$ to the (unperturbed) Fe(II)−Co(III) ground state, which can be seen by inserting the MOs (1 and 2) into the GS wave function (4) and expanding the Slater determinant, giving

$$\Psi^{GS} = (1-\alpha^2)|d_{x^2-y^2}^{+\,Fe}\, d_{x^2-y^2}^{-\,Fe}| - \sqrt{2}\alpha\frac{1}{\sqrt{2}}\{|d_{x^2-y^2}^{+\,Fe}\, d_{xz}^{-\,Co}| - |d_{x^2-y^2}^{-\,Fe}\, d_{xz}^{+\,Co}|\} + \alpha^2|d_{xz}^{+\,Co}\, d_{xz}^{-\,Co}| \approx |d_{x^2-y^2}^{+\,Fe}\, d_{x^2-y^2}^{-\,Fe}| - \sqrt{2}\alpha\frac{1}{\sqrt{2}}\{|d_{x^2-y^2}^{+\,Fe}\, d_{xz}^{-\,Co}| - |d_{x^2-y^2}^{-\,Fe}\, d_{xz}^{+\,Co}|\} \quad (11)$$

Evaluation of V_{AB} and α for 2. Application of the treatment of the previous section to compound **2** is somewhat more involved. The symmetry of the optimized structure **II** is close to C_{2v}. As for compound **1**, the frontier orbitals which have to be considered for the MMCT transition are the HOMO and HOMO−1 as well as the LUMO and the LUMO+1. Both pairs of orbitals are nearly degenerate, having A_1 (HOMO), B_2 (HOMO−1), B_1 (LUMO), and A_2 (LUMO+1) symmetries (cf. Table 3). As mixing between the ground and excited state can only occur within wave functions of the same symmetry, a ground-to-excited-state interaction is impossible for compound **2** in the point group C_{2v}, excluding the possibility of an intense low-energy MMCT transition to account for band I.

Nevertheless, there are two electric-dipole-allowed (ED-allowed) transitions from the HOMO ⟨84⟩ to the LUMO ⟨85⟩, as well as from the HOMO−1 ⟨83⟩ to the LUMO+1 ⟨86⟩, both of which are X-polarized (i.e., in the fulvalenide−fulvalenide direction). In practice, however, the HOMO−1 ⟨83⟩ → LUMO+1 ⟨86⟩ transition will be of vanishing ED intensity as ⟨83⟩ is almost totally localized on the Fe and ⟨86⟩ almost totally on the Co side. Thus only the HOMO−LUMO transition ⟨84⟩ → ⟨85⟩ needs to be considered for band I. To this end, the composition of the HOMO and the LUMO in terms of the subunit orbitals is explicitly formulated[29]

$$\mathrm{HOMO} = \sqrt{1-\xi^2}\, d_{x^2-y^2}^{\,Fe} - \xi d_{x^2-y^2}^{\,Co} \quad (12)$$

and

$$\mathrm{LUMO} = \sqrt{1-\eta^2} d_{xz}^{\,Co} - \eta d_{xz}^{\,Fe} \quad (13)$$

The electric dipole matrix element for the HOMO−LUMO transition within the dimer thus can be expressed as

$$\langle \mathrm{HOMO}|\mu|\mathrm{LUMO}\rangle = \sqrt{1-\xi^2}\sqrt{1-\eta^2}\langle d_{x^2-y^2}^{\,Fe}|\mu|d_{xz}^{\,Co}\rangle - \sqrt{1-\xi^2}\eta\langle d_{x^2-y^2}^{\,Fe}|\mu|d_{xz}^{\,Fe}\rangle - \sqrt{1-\eta^2}\xi\langle d_{x^2-y^2}^{\,Co}|\mu|d_{xz}^{\,Co}\rangle + \xi\eta\langle d_{x^2-y^2}^{\,Co}|\mu|d_{xz}^{\,Fe}\rangle \quad (14)$$

The first and last terms can be neglected because the involved orbitals are located at different metal centers. The matrix elements in the two intermediate terms are about equal

$$\langle d_{x^2-y^2}^{\,Fe}|\mu|d_{xz}^{\,Fe}\rangle \approx \langle d_{x^2-y^2}^{\,Co}|\mu|d_{xz}^{\,Co}\rangle \equiv \langle d_{x^2-y^2}^{\,M}|\mu|d_{xz}^{\,M}\rangle \quad (15)$$

(M = Fe or Co). Omitting quadratic terms, eq 13 thus can be reduced to

$$\langle \mathrm{HOMO}|\mu|\mathrm{LUMO}\rangle \approx -(\xi+\eta)\langle d_{x^2-y^2}^{\,M}|\mu|d_{xz}^{\,M}\rangle \quad (16)$$

Therefore (cf. eq 7)

$$I^{\mathrm{BandI}} = 2(2.511\times10^3\tilde{\nu}_{\max}^{\,I})(\xi+\eta)^2|\langle d_{x^2-y^2}^{\,M}|\mu|d_{xz}^{\,M}\rangle|^2 \quad (17)$$

This expression can be evaluated by comparison with that accounting for the intensity of band II. In the fully symmetric dimer, this absorption feature is the result of the combined, intraMc LF transitions from the $d_{x^2-y^2}/d_{xy}$ set of highest-occupied to the d_{xz}/d_{yz} set of lowest-unoccupied orbitals of the ferrocene and the cobaltocenium subunits. In C_{2v} symmetry, only the $d_{x^2-y^2} \rightarrow d_{xz}$ and the $d_{xy} \rightarrow d_{yz}$ transitions are ED-allowed; therefore

$$I^{\mathrm{BandII}} = 2(2.511\times10^3\tilde{\nu}_{\max}^{\,II})\{|\langle d_{x^2-y^2}^{\,Fe}|\mu|d_{xz}^{\,Fe}\rangle|^2 + |\langle d_{x^2-y^2}^{\,Co}|\mu|d_{xz}^{\,Co}\rangle|^2 + |\langle d_{xy}^{\,Fe}|\mu|d_{yz}^{\,Fe}\rangle|^2 + |\langle d_{xy}^{\,Co}|\mu|d_{yz}^{\,Co}\rangle|^2\} = 2(2.511\times10^3\tilde{\nu}_{\max}^{\,II})\times\{2|\langle d_{x^2-y^2}^{\,M}|\mu|d_{xz}^{\,M}\rangle|^2 + 2|\langle d_{xy}^{\,M}|\mu|d_{yz}^{\,M}\rangle|^2\} \quad (18)$$

The relative intensities of the $d_{xy} \rightarrow d_{yz}$ with respect to the $d_{x^2-y^2} \rightarrow d_{xz}$ transitions are unknown.[32] For an estimate of an upper limit of the intensity of band I, however, it can be stated (assuming $\tilde{\nu}_{\max}^{\,I} \approx \tilde{\nu}_{\max}^{\,II}$)

$$I^{\mathrm{BandI}} \le \frac{(\xi+\eta)^2}{2} I^{\mathrm{BandII}} \quad (19)$$

The values ξ and η as derived from the DFT calculation are 0.12 and 0.34, respectively.[33] In C_{2v} symmetry, the ED intensity of band I thus should be less than 10% of the intensity of band II. As the observed intensity of band I of compound **2** clearly is above this limit, the remaining intensity must be the result of an IVCT-like MMCT transition

Table 3. Symmetries of Involved Frontier Orbitals for the Optimized Structures $FcCc^+$ (**I**) and $BFFeCo^+$ (**II**)

	$FcCcPF_6$ (**1**)	$BFFeCoPF_6$ (**2**)	
	C_s	C_{2v}	C_2 (twisted)
HOMO	A′	A_1	A
LUMO	A′	B_1	B
HOMO−1	A″	B_2	B
LUMO+1	A″	A_2	A

(30) Tuczek, F.; Solomon, E. I. In *Comprehensive Inorganic Chemistry II*; Lever, A. B. P., Ed.; Elsevier: New York, 2003; Vol. 1.
(31) Tuczek, F.; Solomon, E. I. *Coord. Chem. Rev.* **2001**, *219−221*, 1075.
(32) The ED intensity of all of these transitions is the result of the admixture of ligand (cp) orbitals and the loss of inversion symmetry in the coupled system.
(33) These values have been derived from the ratio of the coefficients of the pure Fe and Co d orbitals (see Supporting Information for these values) in the HOMO and the LUMO, assuming that these coefficients are proportional to the coefficients of the corresponding metal−ligand admixed subunit orbitals, in the sense of ref 29.

which *only can occur in a symmetry lower than* C_{2v}. On the basis of the X-ray structure information[13] of compound **2**, we assume that this is the twisted geometry which lowers the symmetry of **2** to C_2. In this point group, the symmetries of the HOMO, HOMO−1, LUMO, and LUMO+1 are modified to A, B, B, and A, respectively, such that totally symmetric excited states result from HOMO → LUMO+1 and HOMO−1 → LUMO transitions (cf. Table 3). The latter interaction will be stronger because of overlap considerations, and correspondingly, the IVCT-like MMCT transition will be more intense. Note that this transition will be Z-polarized (i.e., along the metal−metal vector), in contrast to the ED-allowed HOMO−LUMO transition which is X-polarized (i.e., along the fulvalenide−fulvalenide direction)

For both compound **1** and **2,** the parameters α and V_{AB} therefore can formally be evaluated from eqs 8 and 10, with the understanding that the values obtained for **2** represent upper limits (i.e., some of the intensity of band I in compound **2** may be due to the X-polarized ED-allowed HOMO−LUMO transition, which is not accounted for by this evaluation). For **2**, the metal−metal distance can be taken from the crystal structure[13] (3.879 Å) as the cation is very rigid. For compound **1**, an estimate of *r* is more difficult. Although for bimetallocenic compounds trans configurations have been shown in the solid state,[34] it is possible that in solution a cis configuration is present. In this case, a distribution of *r* values ranging from 3.9 to 5.1 Å would have to be considered, being limited by the possible distances in the cis and trans conformers of **1**. From the solvatochromism of band I, on the other hand, it can be determined that **1** exhibits a trans configuration in solution (see below). Therefore a metal−metal distance of 5.1 Å is applied for the evaluation of α.

The parameters resulting from the analysis of band I are collected in Table 4. The values of the delocalization parameters, α, reflect a small, but significant, communication between the metallocene subunits, with α being larger for the singly bridged dimer than for the doubly bridged dimer. Nevertheless, both systems can be regarded as essentially being localized on the Fe(II)−Co(III) side, in agreement with the NMR, Mössbauer, and magnetic susceptibility data.

Evaluation of Reorganization Energies. According to Hush[18] the optical transition energy

$$E_{op} = hc\tilde{\nu}_{max} \equiv hc\lambda \tag{20}$$

of a symmetric homonuclear mixed-valence system corresponds to the reorganization energy, λ (cf. Figure 6). Introduction of an inequivalency in the coordination spheres leads to the expression

$$\tilde{\nu}_{max} = \lambda + \Delta G^\circ \ (cm^{-1}) \tag{21}$$

where ΔG° is the difference in zero-level energies of the ground and excited electronic state as shown in Figure 6. The value of ΔG° can be estimated from the difference in the redox potentials of the isolated subunits. For the monomeric unsubstituted metallocenes (ferrocene/ferrocenium vs cobaltocene/cobaltocenium) this difference is 1.31 V in acetonitrile and 1.32 V in dichloromethane.[35] Based on these values, the reorganization energies, λ, are 7551 and 4610 cm^{-1} (in acetonitrile solution) for **1** and **2**, respectively. In dichloromethane, λ values of 6596 and 3826 cm^{-1} for **1** and **2**, respectively, are obtained.

The reorganization energy, λ, has an inner-sphere and outer-sphere part[36]

$$\lambda = \lambda_i + \lambda_o \tag{22}$$

The outer-sphere reorganization energy can be evaluated, using a dielectric continuum model for the solvent, according to eq 23 where the values a_1, a_2, and *r* represent the radii of the two redox-active moieties and the distance between them, respectively, and η and D_s are the solvent's refractive index and dielectric constant, respectively

$$\lambda_o = e^2\left(\frac{1}{a_1} + \frac{1}{a_2} - \frac{1}{r}\right)\left(\frac{1}{\eta^2} - \frac{1}{D_s}\right) \tag{23}$$

According to eq 23 there should be a linear relationship between the outer sphere reorganization energy and the solvent function $(1/\eta^2 - 1/D_s)$. As the variation of ΔG° with the solvent is very small,[37] a linear relationship is also

Table 4. Results of the Hush Analysis of the I Bands for $FcCcPF_6$ (**1**) and $BFFeCoPF_6$ (**2**) in Acetonitrile and Dichloromethane[a]

	acetonitrile		dichloromethane	
	$FcCcPF_6$	$BFFeCoPF_6$	$FcCcPF_6$	$BFFeCoPF_6$
$\tilde{\nu}_{max}$ (cm^{-1})/ (ϵ_{max} (M^{-1} cm^{-1}))	18 115 (2480)	15 174 (420)	17 241 (2440)	14 471 (320)
$\Delta\tilde{\nu}_{1/2}$(exptl) (cm^{-1})	4670	5060	4550	4580
ΔG^o (cm^{-1})	10564	10564	10644	10644
λ (cm^{-1})	7551	4610	6596	3826
$\Delta\tilde{\nu}_{1/2}$(theo) (cm^{-1})	4176	3263	3903	2972
V_{AB} (cm^{-1})	1301	671	1243	543
α	0.07	0.04	0.07	0.04

[a] Values of ΔG° were taken from ref 35.

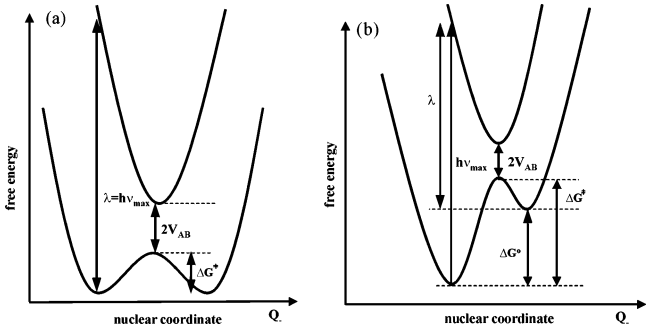

Figure 6. Potential-well diagram representing (a) a symmetrical and (b) an unsymmetrical class II mixed-valent dimer.

(34) MacDonald, A. C.; Trotter, J. *Acta Crystallogr*. **1964**, *17*, 872.

(35) Barlow, S. *Inorg. Chem*. **2001**, *40*, 7047.
(36) Creutz, C. *Prog. Inorg. Chem.* **1983**, *30*, 1.
(37) The electrochemically derived values of ΔG° as taken from ref 35 are nearly solvent independent, therefore a mean value of 10 600 cm^{-1} for ΔG° has been taken.

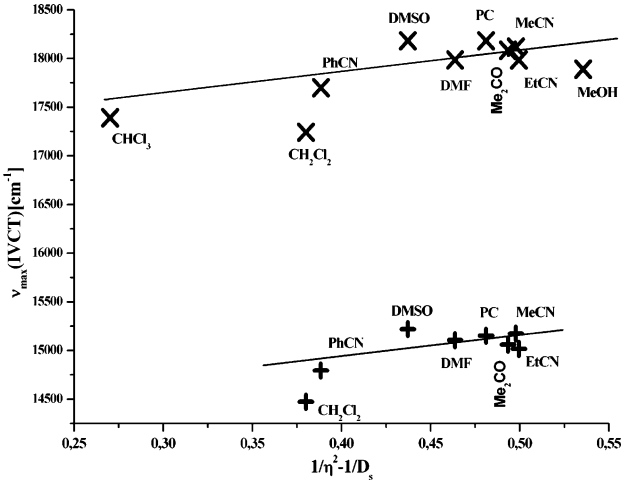

Figure 7. Variation of the maximum of bands I vs solvent function. See text for more details.

expected between $\tilde{\nu}_{max}$ and $(1/\eta^2 - 1/D_s)$, with the intercept corresponding to $\lambda_i + \Delta G°$ (cf. eq 21). Figure 7 shows a plot of the frequency of band I ($\tilde{\nu}_{max}$) versus $(1/\eta^2 - 1/D_s)$ for several solvents.[38] Linear regression analyses[39] of these data give inner-sphere reorganization energies, λ_i, of 6193 cm^{-1} for **1** and 3562 cm^{-1} for **2** (cf. biferrocenium 3530 cm^{-1})[40] and outer-sphere reorganization energies, λ_o, of 1358 and 1048 cm^{-1} for **1** and **2**, respectively.[41]

Within a series of ions having identical a_1 and a_2 values, the slope of the transition energy versus $(1/\eta^2 - 1/D_s)$ is correlated with the distance between the two redox centers. In the case of the very rigid cation $BFFeCo^+$ (**2**), the metal−metal distance can be taken from the crystal structure (vide supra).[13] The linear regression analysis gives a slope of 1959 cm^{-1} for **2**. With a value of 2550 cm^{-1}, the slope is about 1.3 times larger for $FcCc^+$ (**1**). From this information a metal−metal separation of 5.04 Å between the two redox centers of **1** can be inferred. This value is very close to that expected for a trans conformation and has been used in the evaluation of α for compound **1** (vide supra).

In the Hush treatment, finally, the value of λ is related to the theoretical line width of the IVCT band according to

$$\Delta\tilde{\nu}_{1/2(theo)} = \sqrt{2310\lambda} \qquad (24)$$

Gaussian fit analysis of band I reveals experimental line widths of 4670 cm^{-1} for ferrocenyl cobaltocenium hexafluorophosphate (**1**) and 5060 cm^{-1} for ferrocenylene cobaltocenylenium hexafluorophosphate (**2**); both measured in acetonitrile solution.[42] The theoretical values as derived from eq 24 are 4176 and 3263 cm^{-1}, respectively. Thus, in both cases, the theoretical bandwidths are smaller than the experimental values (deviation 10 and 35%, respectively). A possible reason for the larger discrepancy between the theoretical and experimental line widths in **2** could be the fact that band I in this system is the result of a low-symmetry distortion (twisting), giving rise to a distribution of transition energies and therefore an inhomogeneous broadening of the optical absorption band.

III. Discussion

In the preceding sections, the electronic structure and spectroscopic properties of ferrocenyl cobaltocenium PF_6 ($FcCcPF_6$, **1**) and ferrocenylene cobaltocenylenium PF_6 ($BFFeCoPF_6$, **2**) have been determined. On the basis of the results of the Mössbauer and NMR spectroscopy, as well as the magnetic measurements, it is concluded that both $FcCcPF_6$ and $BFFeCoPF_6$ are diamagnetic low-spin Fe(II)−Co(III) d^6−d^6 systems. Nevertheless, there are appreciable electronic interactions within the metallocene subunits of **1** and **2,** which can be inferred from the presence of intermetallocene (interMc) transitions in the VIS/NIR region of their optical absorption spectra (bands I, III, and V). The respective lowest-energy components of these new absorption features, band I, have metal-to-metal CT (MMCT) character and correspond to the IVCT transitions of homonuclear class II mixed-valence (MV) systems. It is shown in this paper that the former bands can be analyzed in a manner similar to that for the latter ones, applying a formalism related to Hush theory.[18] The resulting orbital delocalization parameters, α, and electronic-coupling matrix elements, V_{AB}, are associated with individual orbital interactions in the dimer, analogous to the IVCT transitions of MV systems which provide information on the respective HOMO−SOMO interaction. This way, α parameters of 0.07 and 0.04 are obtained for **1** and **2**, respectively, which reflect the HOMO−LUMO interactions of these systems. In principle, the other interMc bands, III and V, can be analyzed in a similar manner, providing information on other orbital interactions.

The α values obtained from the analysis of the I bands of **1** and **2** are on the same order of magnitude as those found by application of the Hush model for the corresponding diiron (Fe(II)−Fe(III)) cations, biferrocenium ($FcFc^+$, 0.09) and bisfulvalene diiron (BFD^+, 0.09).[43] This is surprising as the Fe(II)−Co(III) systems exhibit large differences in zero-point energies ($\Delta G°$), which are zero in case of the homometallic analogues; a comparable electronic-coupling matrix element, V_{AB}, therefore should lead to much higher α values for the Fe(II)−Fe(III) systems than for the Fe(II)−Co(III). In fact, if a vibronic model (PKS; Piepho, Krausz, Schatz)[44] is employed to analyze the IT bands of $FcFc^+$ and BFD^+ and the resulting λ and ϵ values are converted to α, delocalization parameters of 0.35 and 0.43, respectively, are obtained which are almost 1 order of magnitude larger than those resulting from application of the Hush model.[45] The corresponding λ

(38) The values of η and D_s were taken from the following: (a) Chang, J. P.; Fung, E. Y.; Curtis, J. C. *Inorg. Chem.* **1986**, *25*, 4233. (b) *CRC Handbook of Chemistry and Physics*, 67th ed.; CRC Press, Inc.: Boca Raton, FL, 1987.

(39) Since in dichloromethane solution the observed transition energies in metallocenic systems often show a stronger red shift than the expected one, this value has not been taken into account for the linear regression (ref 1g and references therein).

(40) Powers, M. J.; Meyer, T. H. *J. Am. Chem. Soc.* **1978**, *100*, 4393.

(41) Only the acetonitrile data were taken into account for the known reasons.

(42) In dichloromethane, the bandwidths are significantly smaller.

(43) McManis, G. E.; Nielson, R. M.; Weaver, M. J. *Inorg. Chem.* **1988**, *27*, 1827.

(44) Piepho, S. B.; Krausz, E. R.; Schatz, P. N. *J. Am. Chem. Soc.* **1987**, *100*, 2996.

and ϵ values indicate that $FcFc^+$ and BFD^+ are at the class II−class III borderline and suggest that the Hush model is no longer applicable. Moreover, in contrast to the result obtained by the Hush model, a significantly larger metal−metal interaction is obtained for the doubly bridged Fe(II)−Fe(III) system, compared to the singly bridged one. Similar results have been obtained from a gas-phase photoelectron spectroscopic investigation of biferrocene and bisfulvalene diiron, where it was concluded that $FcFc^+$ and BFD^+ should be described as class III systems in the gas phase.[46] Therefore, α values for strongly coupled MV biferrocene systems based on the Hush model are systematically too small and α values derived from the PKS treatment should be used for comparison with isoelectronic heterobimetallic systems. This might be different for bimetallocene systems with saturated carbon bridging groups which a priori are more localized. In that case, the α value of a heterobimetallic system was in fact found to be in the same order of magnitude as those of related (homobimetallic) diiron systems.[35,47] Regardless of the model applied, however, it appears that electronic interactions in Co(II)−Co(III) bimetallocenes are larger than those in the corresponding Fe(II)−Fe(III) dimers.[43] In summary, the α values for the Fe(II)−Co(III) dimers **1** and **2** are thus smaller than for both the Fe(II)−Fe(III) and Co(II)−Co(III) analogues.

Interestingly, α and V_{AB} were found to be larger for **1** than for **2** (0.07 and 1200 cm^{-1} vs 0.04 and ~600 cm^{-1}, respectively), apparently in contrast to the presence of one bridge in **1** versus two bridges in **2**. Closer examination of the electronic structures of **1** and **2**, however, clarifies the origin of this result: The α value of compound **1** reflects the HOMO−LUMO interaction (i.e., an interaction between $d_{x^2-y^2}{}^{Fe}$ and $d_{xz}{}^{Co}$), which is possible in the C_s symmetry of the dimer. The $BFFeCo^+$ cation of **2** has a higher symmetry (C_{2v}), and direct mixing between the HOMO and LUMO is forbidden. Orbital mixing thus can only occur in the presence of a low-symmetry distortion in compound **2**. From the X-ray crystal structure, this is assumed to be a twist of the complex around the metal−metal axis, leading to C_2 symmetry. This allows the (occupied) $d_{xy}{}^{Fe}$ orbital to interact with the (empty) $d_{xz}{}^{Co}$ orbital. Assignment of band I of compound **2** to the corresponding MMCT transition (as opposed to a LF transition of the fully symmetric dimer) is corroborated by the solvatochromic behavior of this absorption feature. Band III which is found at higher energy for both **1** and **2** equally exhibits solvatochromic behavior but again reflects another orbital interaction (i.e., $cp_{xz}{}^{Fe}-d_{xz}{}^{Co}$ for **1**). Importantly, each of these orbital interactions is associated with a singlet MMCT state which mixes into the electronic ground state with a coefficient of $\sqrt{2}\alpha$, thus giving the Fe(II)−Co(III) closed-shell configuration a small amount of Fe(III)−Co(II) open-shell character (cf. eq 11).

Electrochemical data of mixed-valence compounds often have been considered to obtain information on the magnitude of coupling between the redox centers. The homonuclear bimetallocenes biferrocene and bisfulvalene diiron, for example, show differences in redox potentials of the two iron centers of 0.33 V for the singly bridged and 0.59 V for the doubly bridged compound, indicating a greater stabilization of the cation in the latter system.[48] The differences in the electrode potentials of the corresponding Fe(II)−Co(III) compounds **1** and **2** are 1.58 and 1.64 V, respectively[12] (vs 1.31 V for the isolated metallocenes,[35] vide supra). These data would suggest an electronic interaction within the doubly bridged Fe(II)−Co(III) dimer almost identical to that of the singly bridged one. However, the changes in half-wave potentials are due to different contributions: electronic interactions over the bridge, possible direct metal−metal interactions, and an electrostatic interaction resulting from the charge of the neighboring unit. As the sign and magnitude of the individual components is unknown, this experimental result also may be the result of a cancellation of opposing effects. The optical absorption features analyzed in the present paper, in contrast, allow one to directly assess the strengths of individual orbital interactions in bimetallocenic dimers.

Reorganization energies, λ, of 7600 and 4600 cm^{-1} were found for **1** and **2**, respectively. These values are on the same order of magnitude as those determined for the analogous MV biferrocenes $FcFc^+$ and BFD^+ (5300 and 6600 cm^{-1}, respectively).[49] The same applies to the two separate components of λ, the inner-sphere and outer-sphere (solvational) reorganization energies, λ_i and λ_o, respectively, which can be evaluated by plotting the frequency of band I versus the solvent function $(1/\eta^2 - 1/D_s)$. These data give λ_i values of 6193 and 3562 cm^{-1} and λ_o values of 1358 and 1048 cm^{-1} for **1** and **2**, respectively, which may be compared to those obtained for $FcFc^+$ ($\lambda_i = 3530$ cm^{-1} and $\lambda_o = 1770$ cm^{-1})[40] and BFD^+ ($\lambda_i \approx 6600$ cm^{-1} and $\lambda_o \approx 0$ cm^{-1}).[50] Whereas in all of these cases the major part of the reorganization energy is the inner-sphere part, the absolute λ_i values, as well as their relative magnitudes, for the singly vs the doubly bridged systems on one hand and the Fe(II)/Fe(III) versuas the Fe(II)/Co(III) systems on the other hand are hard to interpret. The fact that λ_o (BFFeCo) is found to be about half as large as λ_o ($FcFc^+$) can be attributed to the twisting of the bisfulvalenide dimer in the ground state which acts to lower the reorganization energy by reducing the degree of localization in the dimer.

In summary, the electronic structure and spectroscopic properties of $FcCc^+$ and $BFFeCo^+$ have been determined. Their optical absorption spectra have been fully assigned, allowing the analysis of the distinct orbital interactions in the dimeric systems. Of particular importance is the lowest-energy component of these transitions (band I) which is associated with the HOMO−LUMO interaction. As a

(45) Talham, D. R.; Cowan, D. O. *Organometallics* **1984**, *3*, 1712.
(46) Lichtenberger, D. L.; Fan, H.-J.; Gruhn, N. E. *J. Organomet. Chem.* **2003**, *666*, 75.
(47) Jones, S. C.; Barlow, S.; O'Hare, D. *Chem. Eur. J.* **2005**, *11*, 4473.
(48) Morrison, W. H., Jr.; Krogsrud, S.; Hendrickson, D. N. *Inorg. Chem.* **1973**, *12*, 1998.
(49) Mueller-Westerhoff, U. T.; Eilbracht, P. *J. Am. Chem. Soc.* **1972**, *94*, 9272.
(50) Since the IVCT band of the bisfulvalenediiron cation has been reported to be nearly solvent independent (see ref 43), the resulting outer-sphere reorganization energy is zero.

consequence of these orbital interactions, the Fe(II)−Co(III) ground states of **1** and **2** get contributions of the corresponding Fe(III)−Co(II) MMCT excited states, which are small ($\alpha^2 < 1\%$ for the HOMO−LUMO excitation). Both dimers, **1** and **2**, thus exhibit a high configurational stability on the Fe(II)/Co(III) closed-shell side, in agreement with the results from magnetic susceptibility measurements and NMR, as well as Mössbauer spectroscopy.

IV. Experimental Section

NMR Spectra. The NMR spectra were recorded at 300 K on a Bruker Avance 400 Pulse Fourier Transform spectrometer operating at a ^{1}H frequency of 400.13 MHz and ^{13}C frequency of 100.62 MHz. Referencing was carried out using TMS as the substitutive standard.

^{57}Fe Mössbauer Spectroscopy. The ^{57}Fe Mössbauer spectroscopy was carried out using a standard transmission geometry Mössbauer setup with a MR260A drive system and a MVT-1000 transducer (both from Wissenschaftliche Elektronik GmbH, Starnberg) in triangular acceleration mode with a 25 mCi ^{57}Co(Rh) source. Temperature was controlled with an ITC502 temperature controller (Oxford Instruments) within a continuous-flow cryostat, CF 506 (Oxford Instruments). Data acquisition card CMCA-550 (Wissenschaftliche Elektronik GmbH, Starnberg) was used for data collection. Calibration was carried out using the inner four lines of the six line pattern of α-iron at room temperature. The spectra were fitted by Lorentzians using the EFFI (Hartmut Spiering, Mainz) software.

UV−Vis Spectra. UV−vis spectra were recorded on a Cary 5 UV−Vis−NIR spectrometer using quartz cuvettes with $d = 1$ cm. Resolution was set to 1 nm.

Elemental Analysis. The elemental analysis was performed using a Euro Vector CHNS−O-element analyzer (Euro EA 3000). Samples were burned in sealed tin containers by a stream of oxygen.

Semiquantitative Microprobe Analyses. The semiquantitative microprobe analyses were performed using a Philips ESEM XL 30 scanning electron microscope equipped with an EDX analyzer.

Mass Spectrometry. A Biflex III (Bruker-Daltonics, Karlsruhe) time-of-flight mass spectrometer was used without any additional matrix.

Density Functional Theory Calculations. Spin-restricted DFT calculations using Becke's three parameter hybrid functional with the correlation functional of Lee, Yang, and Parr (B3LYP)[51,52,53] were performed for the singlet ground states of structures **I** and **II**. The LANL2DZ basis set was used for all calculations. It applies the Dunning/Huzinaga full double-ζ (D95) basis functions[54] on the first row and Los Alamos effective core potentials plus DZ functions on all other atoms.[55,56] Convergence was reached when the relative change in the density matrix between subsequent iterations was less than 1×10^{-8} for single points and optimizations. All computational procedures were used as they are implemented in the Gaussian 98 package.[57] Wave functions were plotted using the visualization program Gaussview 2.1.

Ferrocenyl Cobaltocenium Hexafluorophosphate (1). Compound **1** was prepared according to a slightly modified variation of the method developed by Schwarzhans and Stolz[15] involving a nucleophilic attack of ferrocenyllithium[58] onto cobaltocenium hexafluorophosphate. Removing one hydride from the resulting intermediate with triphenylcarbenium hexaflourophosphate gives the product, which is purified by column chromatography giving a dark powder. MS (TOF): *m*/*z* 373.32. Anal. Calcd for $C_{20}H_{18}PF_6$: C, 46.36; H, 3.50. Found: C, 46.41; H, 3.59. Iron-to-Cobalt ratio by EDX: 1:1. ^{1}H NMR (400 MHz, CD_3CN, 300 K): δ 4.05 (s, 5H), 4.53 (dd, $J \approx 2$ Hz, 2H), 4.71 (dd, $J \approx 2$ Hz, 2H), 5.34 (s, 5H), 5.62 (dd, $J \approx 2$ Hz, 2H), 5.82 (dd, $J \approx 2$ Hz, 2H). ^{13}C NMR (166 MHz, CPD, CD_3CN, 300 K): δ 71.2, 72.5, 74.3, 80.1, 84.3, 100.0.

Ferrocenylene Cobaltocenylenium Hexafluorophosphate (2). Compound **2** was prepared according to the procedure of Schwarzhans and Schottenberger[12] using the bisfulvalenedianion and the THF adducts of the metal chlorides. Further purification was achieved by column chromatography on basic alumina with acetonitrile giving a dark-green air-stable powder after evaporation of the solvent. MS (TOF): *m*/*z* 370.99. Anal. Calcd for $C_{20}H_{16}PF_6$: C, 46.55; H, 3.12. Found: C, 46.51; H, 3.04. Iron-to-Cobalt ratio by EDX: 1:1. ^{1}H NMR (400 MHz, CD_3CN, 300 K): δ 4.24 (dd, $J \approx 2$ Hz, 4H), 5.31 (dd, $J \approx 2$ Hz, 4H), 6.40 (dd, $J \approx 2$ Hz, 4H), 7.10 (dd, $J \approx 2$ Hz, 4H). ^{13}C NMR (166 MHz, CPD, CD_3CN, 300 K) δ 70.0, 80.2, 80.9, 87.6, 128.6.

Acknowledgment. F.T. thanks the State of Schleswig Holstein and FCI for funding of this research.

Supporting Information Available: Detailed discussions of the NMR, Mössbauer, and magnetic characterization, tables of Mössbauer data and d-orbital coefficients, and figures showing ^{1}H NMR and ^{13}C NMR spectra, two dimensional ^{1}H NMR spectra, Mössbauer spectra, Gaussian fit analysis of the UV−vis spectra, and molecular orbital schemes. This material is available free of charge via the Internet at http://pubs.acs.org.

IC051809L

(51) Becke, A. D. *Phys. Rev. A.* **1988**, *38*, 3098.
(52) Becke, A. D. *J. Chem. Phys.* **1993**, *98*, 1372.
(53) Becke, A. D. *J. Chem. Phys.* **1993**, *98*, 5648.
(54) Dunning, T. H., Jr.; Hay, P. J. In *Modern Theoretical Chemistry*; Schaefer, H. F., III, Ed.; Plenum: New York, 1976.
(55) Hay, P. J.; Wadt, W. R. *J. Chem. Phys.* **1985**, *82*, 270 and 299.
(56) Wadt, W. R.; Hay, P. J. *J. Chem. Phys.* **1985**, *82*, 284.
(57) Frisch, M. J.; Trucks, G. W.; Schlegel, H. B.; Scuseria, G. E.; Robb, M. A.; Cheeseman, J. R.; Zakrzewski, V. G.; Montgomery, J. A., Jr.; Stratmann, R. E.; Burant, J. C.; Dapprich, S.; Millam, J. M.; Daniels, A. D.; Kudin, K. N.; Strain, M. C.; Farkas, O.; Tomasi, J.; Barone, V.; Cossi, M.; Cammi, R.; Mennucci, B.; Pomelli, C.; Adamo, C.; Clifford, S.; Ochterski, J.; Petersson, G. A.; Ayala, P. Y.; Cui, Q.; Morokuma, K.; Salvador, P.; Dannenberg, J. J.; Malick, D. K.; Rabuck, A. D.; Raghavachari, K.; Foresman, J. B.; Cioslowski, J.; Ortiz, J. V.; Baboul, A. G.; Stefanov, B. B.; Liu, G.; Liashenko, A.; Piskorz, P.; Komaromi, I.; Gomperts, R.; Martin, R. L.; Fox, D. J.; Keith, T.; Al-Laham, M. A.; Peng, C. Y.; Nanayakkara, A.; Challacombe, M.; Gill, P. M. W.; Johnson, B.; Chen, W.; Wong, M. W.; Andres, J. L.; Gonzalez, C.; Head-Gordon, M.; Replogle, E. S.; Pople, J. A. *Gaussian 98*, revision A.11; Gaussian, Inc.: Pittsburgh, PA, 2001.
(58) Herberhold, M.; Leitner, P. J. *Organomet. Chem.* **1987**, *336*, 153.